SUPPLEMENTARY EXPERIMENTAL PROCEDURES

Recording Methods, Attention Paradigm and Visual Stimulation

Experiments were performed as described in (Fries et al., 2001, 2008). Briefly, spikes and LFPs were recorded from area V4, while monkeys performed a selective attention task. The prelunate gyrus was first localized using magnetic resonance image (MRI) scans. Recording chambers were then implanted over the prelunate gyrus under surgical anesthesia. Before recording through small trepanations of the skull within the recording chamber, four to eight tungsten microelectrodes (impedances of 1-2 MΩ) were advanced separately at a very slow rate (1.5 μm/s) to minimize deformation of the cortical surface by the electrode ('dimpling'). Electrode tips had a fixed horizontal distance of 650 or 900 μm. The median vertical interelectrode spacing was 298 μm with lower (upper) quartiles of the distribution of 144 (585) μm.

The task was structured as follows. A trial started when the monkey touched a bar and directed its gaze within 0.7° of the fixation spot that was presented on the computer screen (onset of fixation period). After approximately 1.5 s, an attentional cue appeared (onset of cue period), which consisted either of a change in color of the fixation spot, or a small line (0.75°) that pointed to the location of the target. For some MUAs and SUA (as specified in the main text), attentional cueing was done in blocks of trials such that the monkey attended to the stimulus inside or outside the receptive field on alternating blocks of trials (Buffalo et al., 2011). The cue was followed after approximately 0.75 s by two drifting grating stimuli (see onset of stimulus period), where one stimulus was cued as the target stimulus and one as the distractor stimulus. The task of the monkey was to release the bar between 150 and 650 ms after a change in color of the target stimulus, i.e. a change of the white stripes of the grating to photometrically isoluminant yellow. Both the target and the distracter stimulus could change color at any unpredictable moment in time between 500 and 5000 ms after stimulus onset, with all times during this period being equally likely for the color change. The color changes were close to the monkeys' detection threshold, ensuring that the task could only be performed when attention was actually allocated to the target. On the 50% of the trials in which the distracter changed before the target, the target nevertheless changed later on in the trial. Those target changes were distributed equally in the remaining time between distracter changes and 5000 ms after stimulus onset. Successful trial completion was rewarded with four drops of diluted fruit juice. If the monkey released the bar before the color change of the target stimulus or if it moved its gaze out of the fixation window, the trial was immediately aborted and followed by a timeout. To select grating stimuli that resulted in strong activation of the recorded units, the following procedure was followed. Before the start of the attention task, direction tuning curves were compiled for all electrodes simultaneously. To this end, a circular patch of drifting square-wave luminance grating (100% contrast, 2-3° diameter, 1-2°/s drift rate, 1-2 cycles/° of spatial frequency) was adjusted in size and location to fit into the region of RF overlap. The orientation of the grating stripes was always orthogonal to the stripes' movement direction, which was varied in steps of 45°. During those measurements, the monkey had to detect a change of the white grating stripes to photometrically isoluminant yellow. At least five repetitions were collected per movement direction. For the selective attention task, we selected the patch of drifting grating that had resulted in maximal coactivation of the simultaneously recorded units. A second patch of drifting grating was placed outside the region of RF overlap. This patch was identical to the inside-RF patch with regard to eccentricity, size, contrast, and spatial and temporal frequency, but its orientation was rotated by 90°. For most recording sessions, the position of the outside-RF patch was 90° away (counterclockwise) from the inside-RF patch at that eccentricity. For a subset of recordings, it was moved to be as close as possible to the RF without evoking a stimulus-driven response.

Data Analysis

All data analysis was performed in MATLAB and using the FieldTrip open source Matlab toolbox (Oostenveld et al., 2011). We analyzed three periods separately: 1.) The fixation period, starting when the monkey attained fixation, and lasting until the onset of the attentional cue; 2.) The cue period, starting from the onset of the attentional cue and lasting until stimulus onset. 3.) The stimulus period, starting with stimulus onset, and lasting until a change in the distracter or the target stimulus, whichever occurred first. The early stimulus period was defined as [0-0.3] s, and the late stimulus period as >0.3 s after stimulus onset.

Offline spike sorting was performed using principal component analysis (Offline Sorter; Plexon). We used the following criteria to include a single unit in our sample: it had to be well isolated from the multi-unit (MUA) on at least one of the first two principal component analysis scores of the waveforms, its isolation had to be stable across time, and a clear refractory period had to be visible in the interspike interval distribution (<0.1% entries in first 1ms bin).

The Spike-LFP Pairwise Phase Consistency (PPC)

For every frequency f, we determined the spike-LFP phases by cutting out LFP segments of length $5/f$ s (i.e., 5 cycles) centered around each spike. Spikes were only related to LFPs recorded from a different electrode to avoid contamination of the LFP by the spike itself. For spikes that fell around the border of an analysis window, we determined the phase of the LFP by cutting out an LFP segment that started at the border of the window, i.e. not centered around the spike. For example, in the context of the cue period analysis, for a spike occurring at -0.01 s before stimulus onset, we determined the gamma phase (50 Hz) (Fig 2E, main text) by cutting out the LFP window ranging from -0.1 to 0 s. This procedure prevented a distortion of the estimated LFP phase by phase resets induced by stimulus onset. The spike-LFP phases

were then obtained as the complex arguments of the Kaiser (with $\beta = 9$) tapered LFP segments. With a Kaiser window, a 50 Hz LFP signal results in -10 dB energy (from leakage) at 30 and 70 Hz, which roughly corresponds to the bandwidth of the gamma-band oscillations studied in this dataset (Fries et al., 2008). For the low-frequency analysis on the complete pre-stimulus period (Figure 2E,F and 4C, 5B, main text), we increased the spectral resolution by using 7 cycles with a Hanning taper, which gives around -10 dB energy at 7.5 and 12.5 Hz for a 10 Hz signal component. We always averaged the spike-LFP phases across the different electrodes (excluding the electrode on which the unit under consideration was recorded) before computing measures of phase consistency.

The strength of spike-LFP phase-locking was quantified by the PPC, which is unbiased by the number of spikes (Vinck et al., 2012, 2010). For the j–th spike in the m-th trial we denote the average spike-LFP phase as $\theta_{m,j}$, where dependence on frequency is omitted in what follows. The PPC is then defined as

$$\hat{\psi} = \frac{\sum_{m=1}^{M} \sum_{l \neq m}^{M} \sum_{j=1}^{N_m} \sum_{k=1}^{N_l} \cos(\theta_{l,k} - \theta_{m,j})}{\sum_{m=1}^{M} \sum_{l \neq m}^{M} N_m N_l} . \qquad (1)$$

The PPC quantifies the average similarity (i.e., in-phaseness) of any pair of two spikes from the same cell in the LFP phase domain. Note that all pairs of spikes from the same trial are removed by virtue of letting $l \neq m$ in eq. 1, because spike phases from the same trial can typically not be treated as statistically independent random variables (Vinck et al., 2012).

While the PPC solves the problem of sample-size bias, PPC estimates are highly variable for units with a low number of spikes (Vinck et al., 2010). To address this problem, we only considered PPC values if they were based on a sample of more than 50 spikes, which can strongly reduce the variance of the group average (Vinck et al., 2010). The variance of PPC estimates is negatively dependent on the number of spikes, and is larger if the expected PPC value is smaller. Consequently, PPC values smaller than zero can occasionally occur in case of weak spike-LFP phase-coupling and low spike counts (Vinck et al., 2010). To obtain PPC spectra with potentially increased signal-to-noise ratio for pre-stimulus periods with weak spike-LFP phase-coupling and low spike counts, we therefore computed so called *weighted PPC group-averages*, defined as

$$\hat{\mu} = \frac{\sum_{s=1}^{S} w_s \hat{\psi}_s}{\sum_{s=1}^{S} w_s} , \qquad (2)$$

where we set $w_s = N_s$, where N_s is the total number of spikes recorded from the s-th cell and $\hat{\psi}_s$ is the estimated PPC for the s-th cell as defined by eq. 1. Because the variance of the PPC estimates is a decreasing function of N_s, a natural choice for w_s is to be an increasing function of N_s. If the expected PPC value would not differ between cells, and PPC estimates would be normally distributed (which holds approximately true for larger spike counts because of the central limit theorem), then weighting by the inverse of the estimator variance would reduce the mean squared error of the mean PPC estimate in comparison to the unweighted PPC average. This dependence on N_s is *a priori* unknown, as it depends on the (unknown) expected PPC value, although our simulations on circular von Mises distributions (data not shown) reveal that for typical PPC values (say below <0.2), it typically decreases at a faster pace than $1/N_s$. The disadvantage of weighting dependent on N_s is that the most active cells may not necessarily be representative of the population, and that the assumption that the cells have the same expected PPC values is likely to be violated (as follows from the rate-PPC correlation presented in Figure 7A-C in the main text), which may lead to a substantial increase in the standard error of the weighted PPC estimate in comparison to the unweighted PPC estimate. Nevertheless, we included the weighted PPC estimate at those places in the manuscript where the spike counts of the analyzed cells were relatively low (Figure 2B, D, and F in main text). This allowed us to examine the robustness of our findings. Note that the unweighted PPC with some threshold on the minimum number of spikes is a special case of eq. 2 with the weights set by the equations $w_s = 1$ for $N_s \geq \tau$ and $w_s = 0$ for $N_s < \tau$, where τ is some threshold, in this case $\tau = 50$. The optimal choice of w_s in eq. 2 is beyond the scope of this manuscript and an open question that will be addressed in future work.

The Network-PPC

To quantify the diversity of spike-LFP phases across cells, we define a new measure that we call the network-PPC. The network-PPC computes the average similarity among spike-LFP phases from a population of cells, and provides an indirect measure for their spike-spike synchronization. The j–th spike of the s–th cell (from S cells) out of N_s spikes fired by that cell is denoted $\theta_{s,j}$. The network-PPC is defined as

$$\hat{\zeta} = \frac{\sum_{s=1}^{S} \sum_{t \neq s}^{S} \hat{\psi}_{s,t}}{S(S-1)} , \qquad (3)$$

where

$$\hat{\psi}_{s,t} \equiv \frac{\sum_{j=1}^{N_s} \sum_{k=1}^{N_t} \cos(\theta_{s,j} - \theta_{t,k})}{N_s N_t} , \qquad (4)$$

quantifies whether the spikes from the s-th and the t-th cell are phase-alligned or not. In fact, a pair of two cells that are firing consistently out of phase contributes a value of -1 to the network-PPC. Network-PPC has the following two properties. 1) Expected value of the network-PPC is unaffected by the number of cells and spike counts in the sample. 2) Across multiple cells, the network-PPC is, on expectation, bound from below by zero. Note the close analogy with eq. 1, expect that we now compute the average similarity among

spike phases from different cells, instead of spike phases from the same cell. The contribution of pairs from the same cell are ignored (just like combinations of spikes from the same trial were ignored in eq. 1), as the measure is designed to capture the consistency of spike phases *among* cells. The contribution of a given pair of spikes is first normalized in eq. 4, and then averaged across all pairs in eq. 3, ensuring that each cell has the same vote in the computation of the network-PPC (however, only units where included for which $N_s > 50$ for a certain condition).

Two cells may have very dissimilar phases, but may still be synchronized at a non-zero phase delay. These phase delays may well be corrected for by axonal delays, such that spikes can arrive in phase at a post-synaptic target. We therefore also introduce a measure called the delay-adjusted network-PPC. This measure is constructed by first rotating the gamma phase distributions such that the preferred phases of any two cells under consideration are aligned, in the sense that their circular means are equal (which is achieved by letting the circular mean direction equal zero for all cells). To be more precise, we compute the mean phase vector $z_s = \sum_{j=1}^{N_s} \exp(i\theta_s)/N_s$, and we then rotate the phases for the s-th cell for every j as $\theta'_{s,j} = \arg(e^{i\theta_{s,j}} z_s^*)$. The *delay-adjusted network-PPC* is then defined by substituting $\theta'_{s,j}$ for $\theta_{s,j}$ in eq. 4, computing the similarity between the phases of any pair of two cells. This yields a pairwise consistency value between 0 and 1 (on expectation). If two cells have no reliable locking to the LFP gamma cycle, then the pairwise consistency value will be zero on expectation, if they are perfectly synchronized to the LFP gamma cycle, then the pairwise consistency will indicate that they are perfectly synchronized (output 1). Importantly, the delay-adjusted network-PPC provides an upper bound to the network-PPC: The delay-adjusted network-PPC quantifies the similarity among spike-LFP phases in the population of cells *as if* all cells had the same preferred phase relative to the LFP. Hence, the degree to which the network-PPC differs from the delay-adjusted network-PPC provides a measure of phase diversity in the population. However, the delay-adjusted network-PPC has some positive sampling bias, in the sense that it tends to output higher values for small spike counts. To see this, consider the case where all cells have uniformly distributed phases. In this case, the rotation of the phases will cause some allignment of the phases on average; this contribution disappears as the number of spikes grows large. This sampling bias is larger if cells have less reliable phase distributions. We therefore implement a conservative bias subtraction by estimating the delay-adjusted network-PPC for the case where all phases were drawn from uniform distribution, using the same number of spike counts. That is, we compute the network PPC according to eq. 3 and substitute $\theta_{s,j}$ by a random variable that is uniformly distributed on the unit circle. An estimate of the expected value of the bias is then derived by repeatedly drawing $\theta_{s,j}$ and averaging across realizations. The resulting bias term is then subtracted from the delay-adjusted network-PPC. Because of this conservative bias correction, the delay-adjusted network PPC tends to be slightly under-estimated. We would like to point out that, in general, the network-PPC is a potentially much more sensitive measure of rhythmic neuronal synchronization in the local population than the average single-cell PPC, as the number of available spike pairs scales with S^2N^2 (with S the number of cells) in eq. 3, rather than with SN^2 for the mean PPC as defined in eq. 1.

The rationale behind the network PPC and the delay-adjusted network PPC is as follows. Suppose we observe a group of neurons ($s = 1, .., S$) with spike counts N_s, PPCs ψ_s, and preferred phases θ_s. The problem can be formulated as providing a measure of the dispersion of θ_s independent of N_s and ψ_s. The circular ANOVA 1) merely provides a statistical decision but does not inform about effect size, and 2) has more statistical power when N_s and ψ_s are large. The network PPC is, by construction, independent of N_s but is still influenced by ψ_s, being lower when the individual PPC's are small, or when the dispersion of the preferred angles is large. The value of the delay-adjusted PPC is only influenced by the PPC's, as the differences in preferred angles are corrected for. Thus, by comparison of the delay-adjusted network PPC and the network PPC, the dispersion of the preferred angles can be gauged from the difference or ratio of network-PPC to delay-adjusted network-PPC. The network-PPC and delay-adjusted network-PPC also have a potential physiological interpretation: network-PPC provides a direct measure of synchronization strength for a population (in terms of alignment of spikes to an oscillatory cycle) when the delays are not corrected for, while delay-adjusted network-PPC does the same but while assuming that the delays are corrected for.

In case of using the network PPC for the combination of SUA and same-site MUA, we did the following. For the s-th cell, let $\theta_{s,j,1}$ represent the phases for the SUA firing $N_{s,1}$ spikes and $\theta_{s,k,2}$ the phases for the same-site MUA firing $N_{s,2}$ spikes. We then computed the network PPC according to $\hat{\zeta} = \frac{1}{S}\sum_{s=1}^{S} \hat{\psi}_s$ where

$$\hat{\psi}_s \equiv \frac{\sum_{j=1}^{N_{s,1}} \sum_{k=1}^{N_{s,2}} \cos(\theta_{s,j,1} - \theta_{s,k,2})}{N_{s,1} N_{s,2}} \tag{5}$$

Spike-triggered LFP-Phase Homogeneity

We also defined a measure called *spike-triggered LFP phase homogeneity*; this measure was defined in close analogy to the network-PPC. For a given pair of LFP channels (from a different electrode than the unit was recorded from), we denote the $j-$th spike-phase in the $m-$th trial for the $c-$th channel as $\theta_{c,m,j}$. The spike-triggered LFP phase homogeneity was then defined as

$$\hat{\psi}_{c,d} \equiv \frac{\sum_{m=1}^{M} \sum_{l\neq m}^{M} \sum_{j=1}^{N_m} \sum_{k=1}^{N_l} \cos(\theta_{c,m,j} - \theta_{d,l,k})}{\sum_{m=1}^{M} \sum_{l\neq m}^{M} N_m N_l} \tag{6}$$

and closely follows the definition of the network PPC in eq. 3. This value was then averaged across the different

LFP channel combinations as

$$\hat{\psi}_s = \frac{\sum_{c=1}^{C}\sum_{d\neq c}^{C}\hat{\psi}_{c,d}}{C(C-1)} \quad (7)$$

and subsequently averaged across cells. Note that, by this definition, two spikes from the same trial are never compared, but that all comparisons of spike-LFP phases run across different trials, similar to the definition in eq. 1. The reason for this is to avoid statistical dependencies that occur in the same trial. The spike-triggered LFP phase homogeneity quantifies to what extent the distribution of spike-LFP phases measured relative to one (LFP) electrode is similar to the distribution of spike-LFP phases measured relative to another (LFP) electrode. The delay-adjusted spike-triggered LFP phase homogeneity is then again defined by rotating phases for every channel such that the circular mean angles equal zero, and again corrected for positive sampling bias, using a similar procedure as for the network PPC.

Statistics on PPC

For correlational analyses in which PPC values were involved, we used Spearman correlations, which are more appropriate given the non-normal distribution of PPC values. Throughout the manuscript, we typically used bootstrap or randomization tests given the non-normal distribution of PPC values, to avoid making assumptions associated with standard parametric tests. We utilize bootstrap tests to test whether some parameter (e.g., the PPC or a difference in PPC between two paired samples or conditions) significantly differs from zero by checking whether the test statistic exceeds the 95% (one-sided, in case of testing PPC against $H_0 : \mu_{\mathrm{PPC}} = 0$) percentile or 97.5% (two-sided, in case of testing difference in PPCs between conditions against $H_0 : \mu_{\Delta\mathrm{PPC}} = 0$) percentile. We utilize randomization testing to see whether an observed difference in some parameter (e.g., a difference in PPC between two samples that are not paired) is significant.

For analyses examining the distributions of the preferred phase of locking (Fig 4 and Fig 5E-F in main text), we only considered those units for which the PPC exceeded zero, i.e. those units for which there was some consistency of phases around a circular mean direction.

Analysis of LFP Power and LFP-LFP Coherence

We analyzed the LFP separately for the higher and the lower frequencies. We first divided the data in 500 ms segments and multi-tapered the LFP segments, using a resolution of ±14 Hz, as in (Fries et al., 2008). For the lower frequencies, we used a single Hann taper, as in (Fries et al., 2008). Denote the cross-spectrum between two channels of the k-th segment out of K segments by X_k. The WPLI (weighted phase lag index) (Vinck et al., 2011) is a measure of phase-synchronization that is not spuriously increased by volume-conduction and is expected to have reduced noise sensitivity relative to previous measures of phase-synchronization that utilize the imaginary part of the cross-spectrum (Nolte et al., 2004; Stam et al., 2007). In addition, we have shown that even in case of two dependent (interacting) sources and sensors, the position of the sources relative to sensors (i.e., the specific volume-conduction mixing coefficients) does not alter the WPLI (Ewald et al., 2012; Vinck et al., 2011). The debiased WPLI estimator is defined as

$$\hat{\phi} = \frac{\sum_{k=1}^{K}\sum_{j\neq k}^{K}\Im\{X_k\}\Im\{X_j\}}{\sum_{k=1}^{K}\sum_{j\neq k}^{K}|\Im\{X_k\}\Im\{X_j\}|} \quad (8)$$

and is a nearly unbiased estimator of the square of the WPLI statistic, which is defined

$$\mathrm{WPLI} = \frac{\mathrm{E}\{\Im\{X\}\}}{\mathrm{E}\{|\Im\{X\}|\}} \quad (9)$$

where X is a random variable identically distributed to X_j for all j. The (debiased) WPLI estimates were then averaged across all channel-combinations.

For the power spectrum, we normalized the power spectrum relative to the average power spectrum (i.e., averaged across all measured frequencies) of the fixation period. That is, if we denote the average power at frequency f in the fixation period by $P(f)$, then we normalized the power spectrum for the higher frequency analysis by $\sum_{f=1}^{F} P(f)$.

References

Buffalo, E. A., Fries, P., Landman, R., Buschman, T. J., & Desimone, R. (2011). Laminar differences in gamma and alpha coherence in the ventral stream. Proc. Natl. Acad. Sci. U.S.A., 108, 11262–11267.

Ewald, A., Marzetti, L., Zappasodi, F., Meinecke, F. C., & Nolte, G. (2012). Estimating true brain connectivity from EEG/MEG data invariant to linear and static transformations in sensor space. Neuroimage, 60, 476–488.

Fries, P., Reynolds, J. H., Rorie, A. E., & Desimone, R. (2001). Modulation of oscillatory neuronal synchronization by selective visual attention. Science, 291, 1560–1563.

Fries, P., Womelsdorf, T., Oostenveld, R., & Desimone, R. (2008). The effects of visual stimulation and selective visual attention on rhythmic neuronal synchronization in macaque area V4. J. Neurosci., 28, 4823–4835.

Nolte, G., Bai, O., Wheaton, L., Mari, Z., Vorbach, S., & Hallett, M. (2004). Identifying true brain interaction from EEG data using the imaginary part of coherency. Clin Neurophysiol, 115, 2292–2307.

Oostenveld, R., Fries, P., Maris, E., & Schoffelen, J. M. (2011). FieldTrip: Open source software for advanced analysis of MEG, EEG, and invasive electrophysiological data. Comput Intell Neurosci, 2011, 156869.

Stam, C. J., Nolte, G., & Daffertshofer, A. (2007). Phase lag index: assessment of functional connectivity from multi channel eeg and meg with diminished bias from common sources. Human brain mapping, 28, 1178–93.

Vinck, M., Battaglia, F. P., Womelsdorf, T., & Pennartz, C. (2012). Improved measures of phase-coupling between spikes and the Local Field Potential. J Comput Neurosci, 33, 53–75.

Vinck, M., Oostenveld, R., van Wingerden, M., Battaglia, F., & Pennartz, C. M. (2011). An improved index of phase-synchronization for electrophysiological data in the presence of volume-conduction, noise and sample-size bias. Neuroimage, 55, 1548–1565.

Vinck, M., van Wingerden, M., Womelsdorf, T., Fries, P., & Pennartz, C. M. (2010). The pairwise phase consistency: a bias-free measure of rhythmic neuronal synchronization. Neuroimage, 51, 112–122.

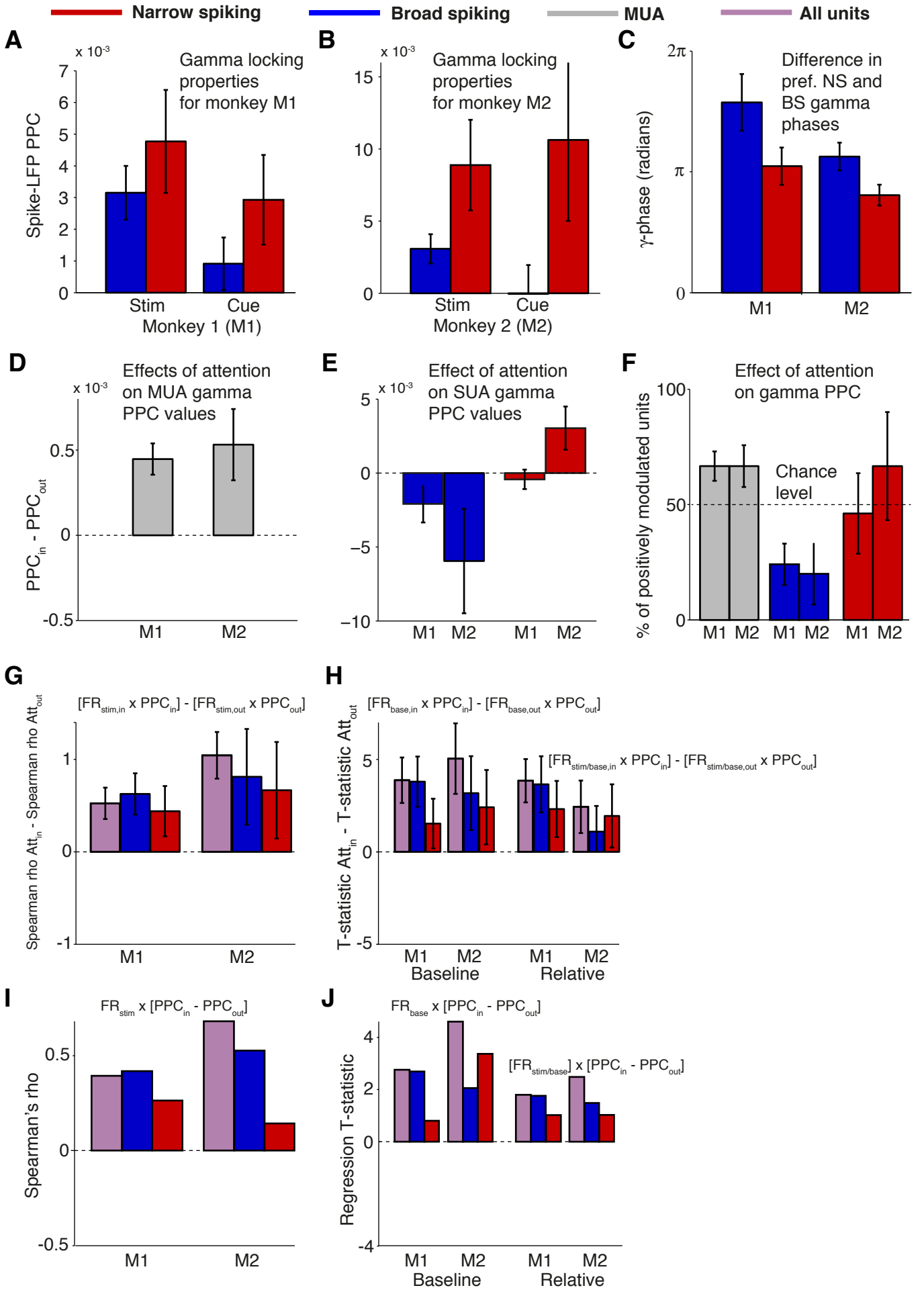

Figure S1. For caption see next page.

Figure S1. Overview of Main Effects, Separately for Monkeys M1 and M2, Related to Figs 1-4 and Figs 6-7.
(A) Mean ± SEM of PPC values for monkeys M1 and M2 at 50 Hz, during sustained stimulus period (see also Fig S2). (B) Mean ± SEM of cue period PPC values for monkeys M1 and M2 at their respective gamma peaks of 40 and 60 Hz during the cue period (see Fig S3). (C) Mean gamma phase for monkeys M1 and M2, at 50 Hz. Error bars indicate 72% confidence intervals. (D) Effect of attention on MUA-LFP gamma PPC values, measured as $PPC_{in} - PPC_{out}$. Shown are means ± SEMs for the 60 Hz bin at which the effect of attention was strongest for both monkeys (see Fig S5G and J). (E) Effect of attention on SUA-LFP gamma PPC values, at the 50 Hz bin, measured as $PPC_{in} - PPC_{out}$. Shown are means ± SEM (see also Fig S5). (F) Percentage of sites for which the gamma PPC value is positively modulated with attention, shown for the 54 Hz bin at which both the BS cells and MUAs reach statistical significance when pooling both monkeys together (see Main text, Fig 6A; see also Fig S5). (G) Difference between attention conditions in Spearman correlations of PPC and stimulus period firing rate, at 50 Hz. Error bars indicate SEMs (see also Fig S6A and Fig S7A). (H) Same as (G), but now shown the difference between attention conditions in the T-statistic of the baseline firing rate predictor, and relative stimulus firing rate to baseline predictor. This T-statistic was derived from a multiple regression of PPC onto baseline firing rate and the relative stimulus firing rate to baseline (see also Fig S6B-C and Fig S7B-C). (I) Spearman correlation between stimulus driven firing rate and the attentional modulation of SUA gamma PPC [$PPC_{in} - PPC_{out}$] for 50 Hz bin (see also Fig S6D and Fig S7D). (J) Same as (I), but now shown the T-statistic of the baseline firing rate predictor, and the T-statistic of the relative stimulus firing rate to baseline predictor (see also Fig S6E-F and Fig S7E-F).

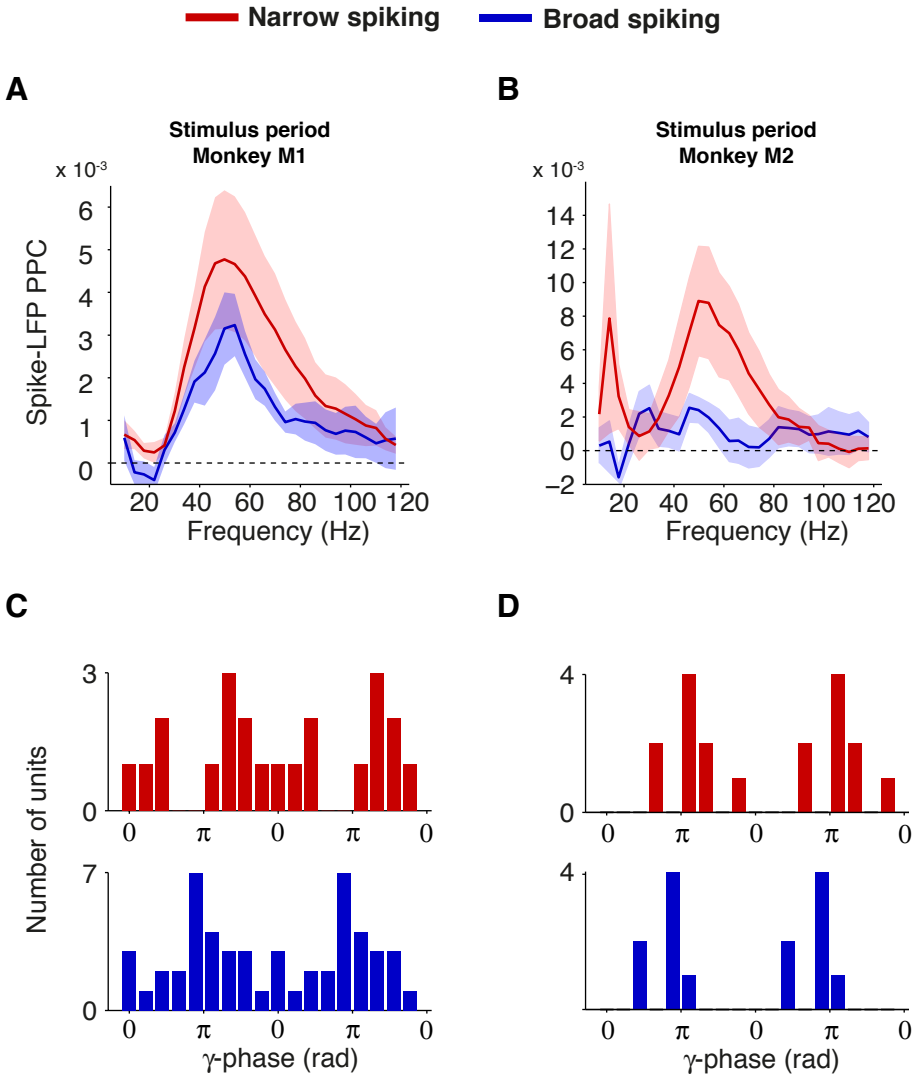

Figure S2. Basic Phase Locking Properties of NS and BS Cells, Separately for Monkeys M1 and M2, Related to Figs 1 and 4.

(A) Sustained stimulation: Average spike-LFP PPC (eq. 1) spectra for monkey M1 (N_{NS} = 13, N_{BS} = 29). (B) Same as (A), but for monkey M2 (N_{NS} = 9, N_{BS} = 10). (C) Histogram of mean spike-LFP gamma phases across units for monkey M2. Only units for which the gamma PPC exceeded zero are shown. NS cells fired at later phase (283.5 ± 89.9°, 95% c.i.) than BS cells (188.5 ± 57.8°, $p < 0.05$, Circular ANOVA). (D) Same as (C), but now for monkey M2. NS cells fired at later phase (202.8 ± 40.17°) than BS cells (145.34 ± 29.05°, $p < 0.05$, Circular ANOVA).

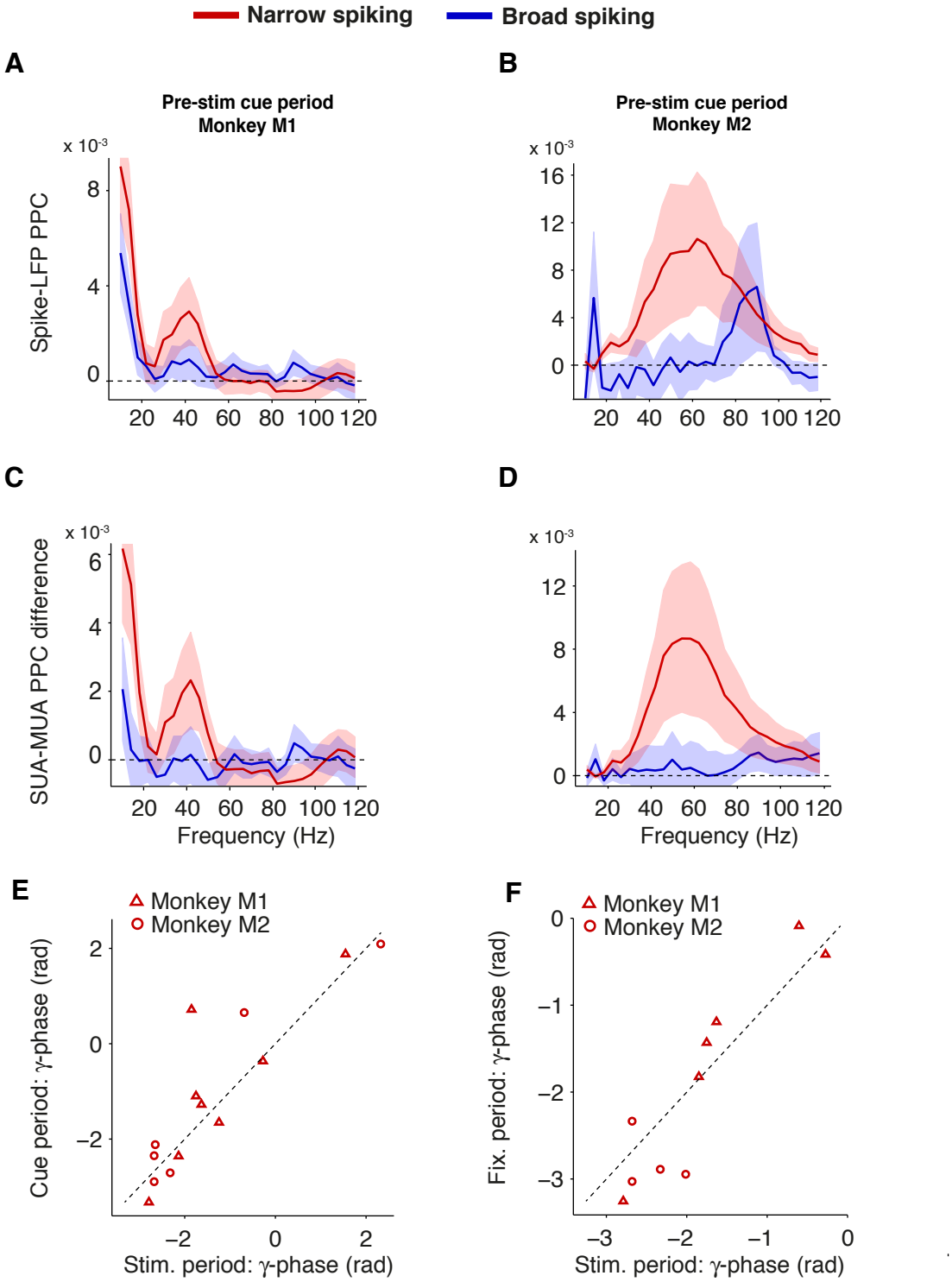

Figure S3. Strength and Phase of Locking in Pre-Stimulus Period for Monkeys M1 and M2 Separately, Related to Figs 2-3 and 5.

(A) Monkey M1: Spike-LFP PPC spectra for cue period (N_{NS} = 12, N_{BS} = 27). (B) Same as (A), but for monkey M2 (N_{NS} = 9, N_{BS} = 10). (C) Same as (A), but now shown the SUA-MUA PPC difference. (D) Same as (C), but now for monkey M2. (E) Mean gamma phase in stimulus period vs. cue period, for NS cells with a spike-LFP PPC exceeding zero in both periods. Triangles and circles correspond to monkey M1 and monkey M2 units, respectively. (F) Same as (E), but now for stimulus period vs. fixation period. (E-F) BS cells were not included for this analysis because these cells did not reliably gamma phase lock in pre-stimulus period (Fig S1).

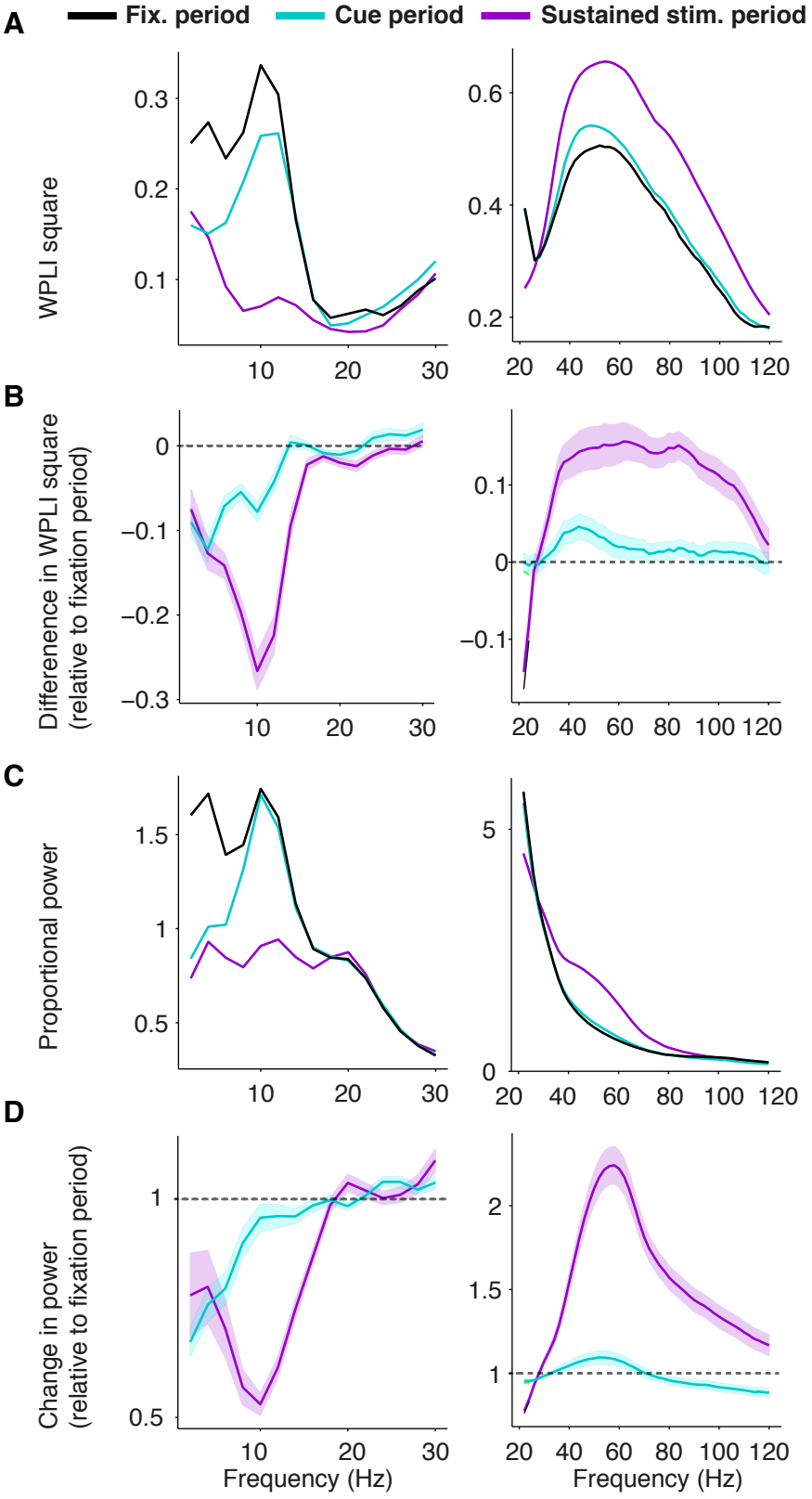

Figure S4. Comparison of LFP Coherence [WPLI] and Power between Fixation, Cue and Sustained Visual Stimulation Period, Related to Figs 2-3.

(A) Spectrum of debiased WPLI (eq. 8) as a function of frequency, separately for low (left panel) and high (right panel) frequencies, revealing a clear gamma-band in the pre-stimulus period. (B) Change in debiased WPLI relative to fixation period [$WPLI_{cue}$ - $WPLI_{fixation}$] and [$WPLI_{stim}$ - $WPLI_{fixation}$]. Shaded regions correspond to SEMs. (C) Power spectrum (normalized by summed power across all plotted frequencies during fixation period). (D) Change in power spectrum relative to the fixation period [$Power_{stim}$ / $Power_{fixation}$] and [$Power_{cue}$ / $Power_{fixation}$]. Shaded regions correspond to SEMs.

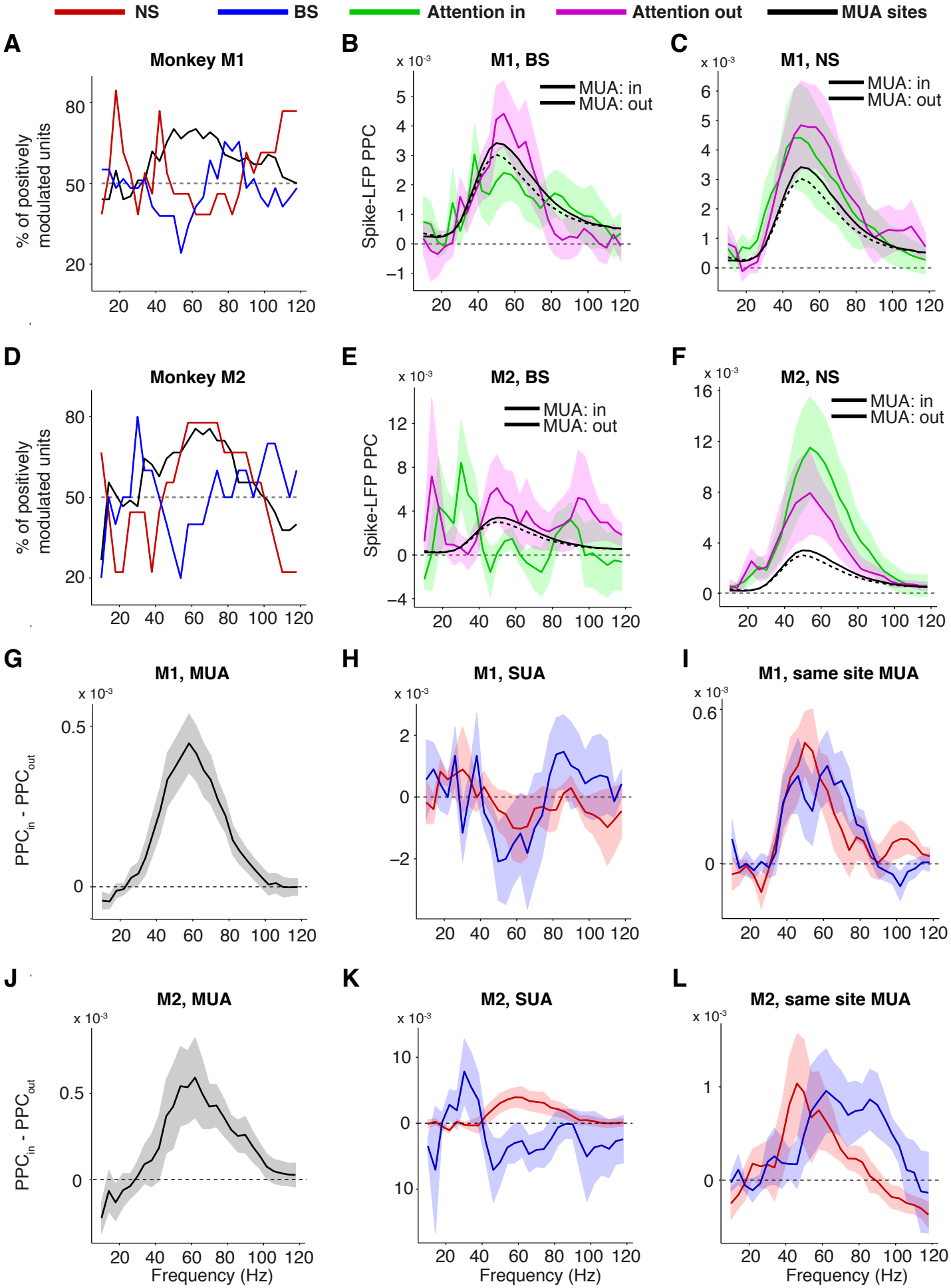

Figure S5. For caption see next page.

Figure S5. Effect of Selective Attention on PPC for Monkeys M1 and M2 Separately, Related to Fig 6.

Same as main text Figure 6, but panels have been reorganized and are shown for the two monkeys separately. (A) Monkey M1: Percentage of SUAs (red, blue) and MUAs (black) for which the gamma PPC was higher with attention inside than outside the RF (N_{NS} = 12, N_{BS} = 29, N_{MUA} = 85). (B) Monkey M1: Average BS cell PPC vs. frequency, separately for attention inside and outside the RF. Solid black and dashed black line correspond to MUA PPC with attention inside and outside the RF, respectively. (C) Same as (B), now for NS cells. (D-F) Same as (A-C), but for monkey M2 (N_{NS} = 9, N_{BS} = 10, N_{MUA} = 45). (G) Monkey M1: Frequency vs. the average difference in MUA-LFP PPC between attention inside and outside the RF. (H) Same as (G), but now for NS and BS cells. (I) Same as (G), but now for the same-site MUAs corresponding to either the NS (red) or BS (blue) cells. (J-L) Same as (G-I), but now for monkey M2. (A-L) Shadings indicate SEMs.

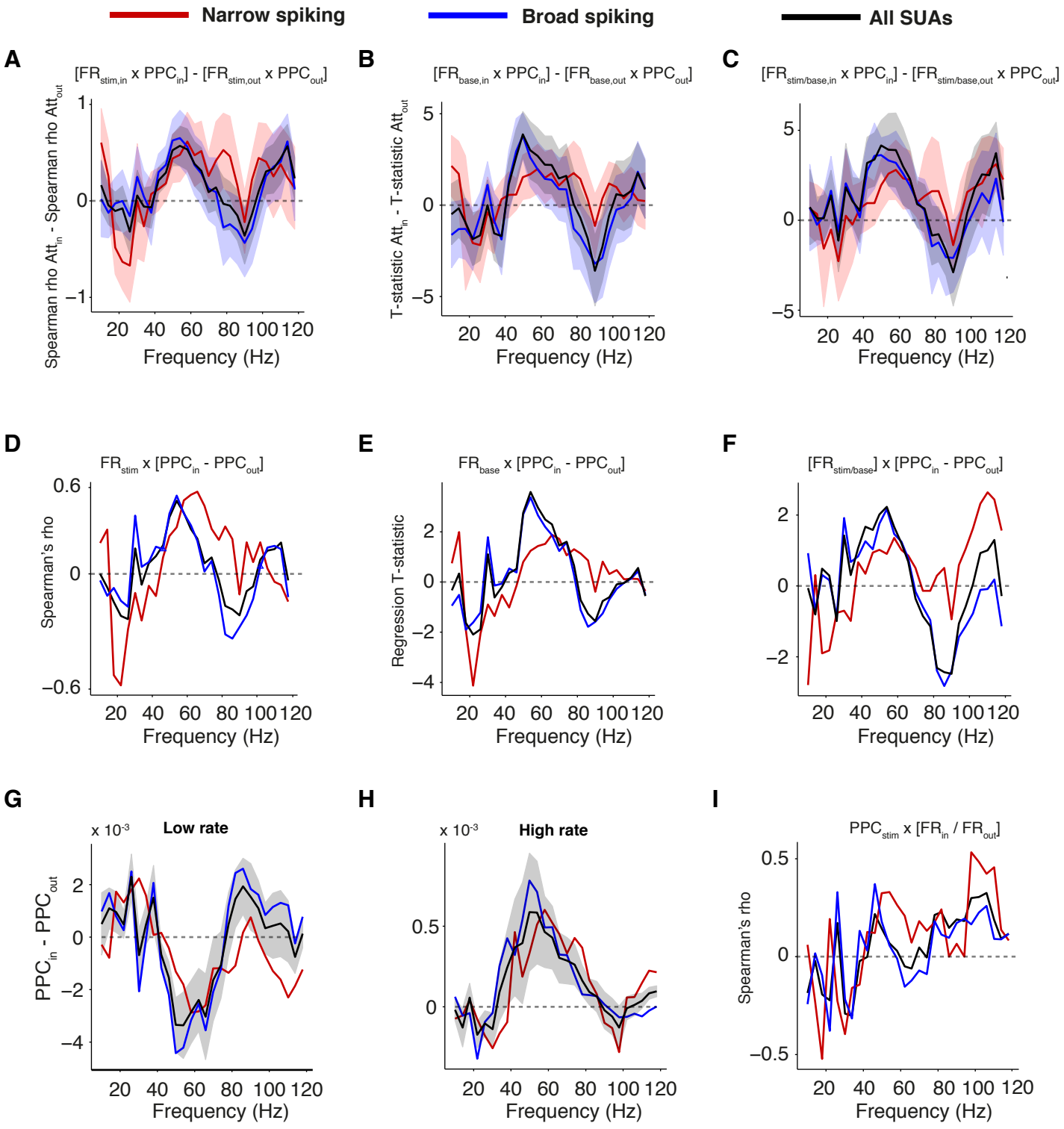

Figure S6. Relationships between PPC, Firing Rate and Selective Attention for Monkey M1, Related to Fig 7.
Same as main text Figure 7, but now for monkey M1 (N_{NS} = 12, N_{BS} = 29). (A) Difference between attention conditions in Spearman correlations of PPC and stimulus period firing rate. Shadings indicate SEMs. (B) Same as (A), but now shown the difference between attention conditions in the T-statistic of the baseline firing rate predictor. This T-statistic was derived from a multiple regression of PPC onto baseline firing rate and relative stimulus firing rate to baseline. (C) Same as (B) but now for the relative stimulus firing rate to baseline. (D) Spearman correlation between stimulus driven firing rate and the attentional modulation of SUA gamma PPC [$PPC_{in} - PPC_{out}$] vs. frequency. (E) Same as (D), but now shown the T-statistic of the baseline firing rate predictor. (F) Same as (E), but now for relative stimulus firing rate to baseline. (G-H) Average difference in PPC between attention conditions for units with low (G) and high (H) average firing rate (median split). (I) Spearman correlation between PPC and attentional modulation of SUA firing rate [FR_{in}/FR_{out}] vs. frequency.

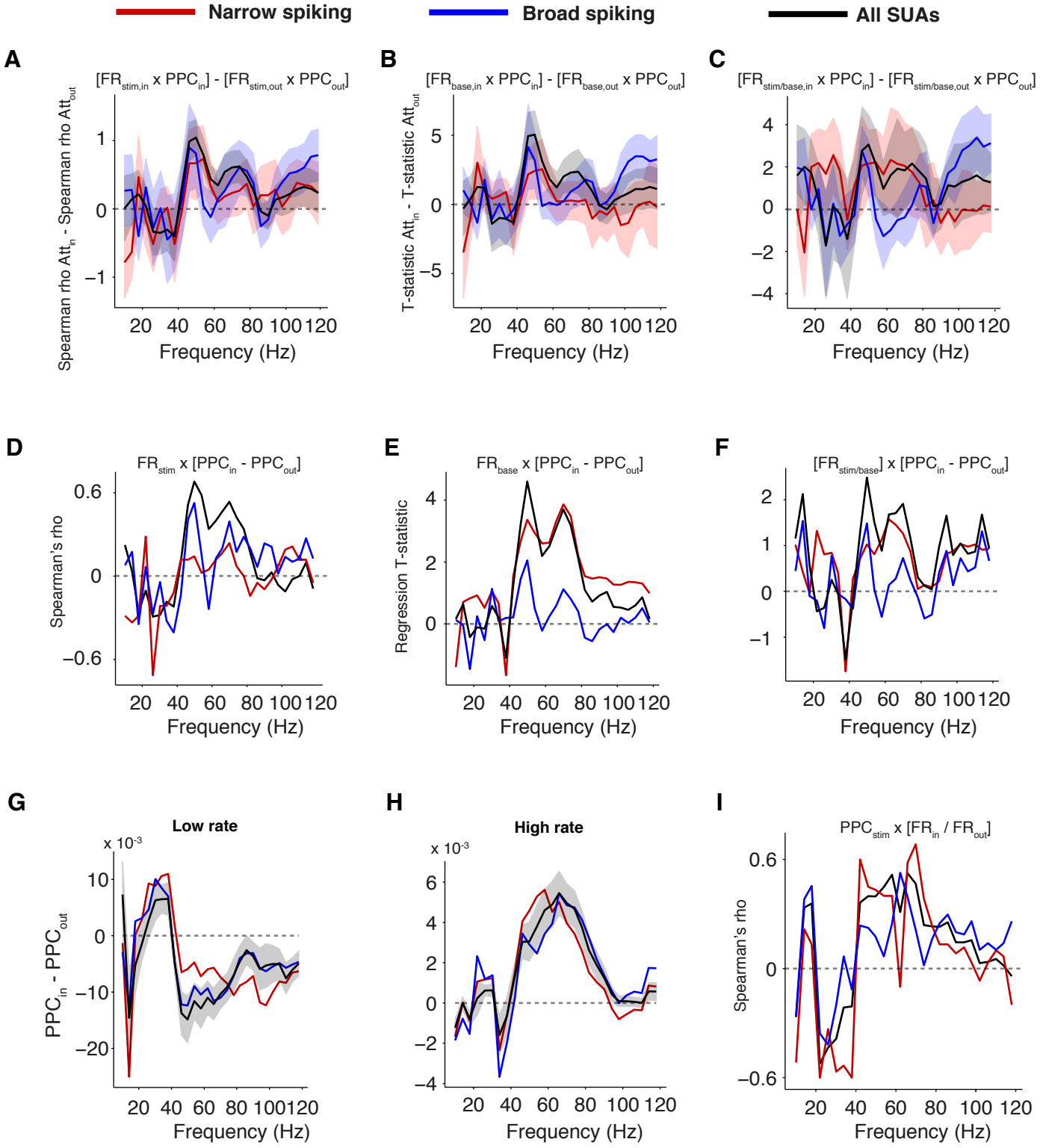

Figure S7. Relationships between PPC, Firing Rate and Selective Attention for Monkey M2, Related to Fig 7.
Same as main text Figure 7, but now for monkey M2 (N_{NS} = 9, N_{BS} = 10). (A) Difference between attention conditions in Spearman correlations of PPC and stimulus period firing rate. Shadings indicate SEMs. (B) Same as (A), but now shown the difference between attention conditions in the T-statistic of the baseline firing rate predictor. This T-statistic was derived from a multiple regression of PPC onto baseline firing rate and relative stimulus firing rate to baseline. (C) Same as (B) but now for the relative stimulus firing rate to baseline. (D) Spearman correlation between stimulus driven firing rate and the attentional modulation of SUA gamma PPC [$PPC_{in} - PPC_{out}$] vs. frequency. (E) Same as (D), but now shown the T-statistic of the baseline firing rate predictor. (F) Same as (E), but now for relative stimulus firing rate to baseline. (G-H) Average difference in PPC between attention conditions for units with low (G) and high (H) average firing rate (median split). (I) Spearman correlation between PPC and attentional modulation of SUA firing rate [FR_{in}/FR_{out}] vs. frequency.